Arc Welding Process Control based on Back Face Thermography: Application to the Manufacturing of Nuclear Steam Generators

A. Cobo, J. Mirapeix, O. M Conde, P.B. García-Allende, F. J. Madruga, J.M. López-Higuera
Photonics Engineering Group, Univ. de Cantabria, Avda. Los Castros s/n, 39005 Santander, Spain

ABSTRACT

The possibility of reducing defects in the arc welding process has attracted research interest, particularly, in the aerospace and nuclear sectors where the resulting weld quality is a major concern and must be assured by costly, time-consuming, non-destructive testing (NDT) procedures. One possible approach is the analysis of a measurand correlated with the formation of defects, from which a control action is derived. Among others, the thermographic analysis of the weld pool and the heat-affected zone have proven to be a useful technique, since the temperature profile of the material being welded has a clear correlation with the process parameters. In this paper, we propose a control system for the submerged-arc welding (SAW) process, based on thermographic imaging of the back face of the joint being welded. In-lab experiments, with simultaneous infrared and a visible imaging, have been performed. Two image analysis techniques are proposed: tracking of the maximum temperature point of the infrared images, and morphological analysis of the visible images. In-lab welding experiments have demonstrated the feasibility of both techniques. They are able to obtain an estimation of the surface temperature and to detect the occurrence of the perforation defect, what has major application for defect detection and reduction in the joining of shell sections of nuclear steam generators.

Keywords: arc-welding, infrared thermography

1. INTRODUCTION

Arc welding is a joining procedure that has been used for years in many industrial applications. In some of them, like the nuclear and aerospace sectors, control quality of the welding process is a major concern. Commonly, off-line, non-destructive testing techniques (x-rays, penetrant liquids, magnetic particles, ultrasonics, etc.) are used to identify defective welds; but these techniques are time-consuming and expensive, and a particular weld seam identified as non-valid would have to be reworked. A real-time sensing and control system could prevent or reduce possible defects, thus reducing costs and improving productivity.

Many principles have been employed for process monitoring, such as measurement of the charge voltage induced on the welding nozzle [1] or analysis of acoustic emissions [2]. Optical methods include measurement of the light emission with remote photodiodes [3] or spectroscopic analysis of the plasma [4].

One particular interesting approach is based on infrared thermography [5-6]. When applied to the arc welding monitoring, the spatial distribution along the surface of the piece to be welded can be obtained. Thus, the size and shape of the welding pool can be inferred [7-9]. Perturbations of the measured temperature have been associated with defects [10-13].

Some drawbacks of this technique are the high cost of infrared thermographic cameras, the real-time requirements for the image processing algorithms, and the infrared radiation coming from the plasma, that is combined with the one emitted by the workpiece surface.

To a lesser extent, visible cameras have been employed for this task. The laser welding process, for example, allows co-axial configurations [14-15], and results with CMOS [16] and CCD [17] cameras have been reported. Visible cameras have been also used for the monitoring of the arc welding process [18, 19]. The main drawbacks of monitoring with visible cameras are the large dynamic range involved the strong electromagnetic interferences from the arc and the environment, and the strong plasma emission from the arc, that needs to be filtered out.

Thermosense XXIX, edited by Kathryn M. Knettel, Vladimir P. Vavilov, Jonathan J. Miles,
Proc. of SPIE Vol. 6541, 65410F, (2007) · 0277-786X/07/$18 · doi: 10.1117/12.718949

If the back face of the pieces being welded is monitored, however, some of these problems are eliminated or mitigated. In particular, the process of submerged arc welding is especially suitable for this approach, because plasma emission from the arc is not accessible, and some of the alternative techniques described (such as plasma spectroscopy or direct imaging of the weld pool) are note feasible.

In the next section, the main characteristics and monitoring needs of the submerged arc welding process, for which this work is intended, are presented.

2. SUBMERGED ARC WELDING PROCESS

The Submerged Arc Welding (SAW) process is commonly used in many industrial sectors for joining ferrous or nickel-based alloys, when a high deposition rate and deep welds are needed. In this process, the electrode is consumable, while the melted material is protected from atmospheric gases by being submerged under a layer of a granulated compound, the welding flux.

This work is focused on the monitoring and control of the welding process of large steam generators for the nuclear industry. In particular, the joining of the outer shell sections of the generators, which is based on a multipass SAW process. Figure 1 shows a scheme of this particular setup. In this Figure, a cross section of the generator is shown. The welding torch (upper part of the figure) is fixed, while the entire workpiece to be welded is rotating along its axis. Typical diameters of the workpiece are 4 or 5 meters, while the thickness of the outer shell can be 10cm or even thicker. To completely join such a thick piece, several passes are required. It must be noted that an initial weld seam only a few millimeter thick is deposited on the internal face of the join, by means of a manually operated Tungsten Inert Gas (TIG) process. This weld seam prevents the two pieces from moving with respect to each other during the first pass. The presence of this initial weld seam, along with the nature of the process itself, prevent a direct vision of the arc or the upper surface of the heat affected zone (HAZ), thus precluding the use of most of the monitoring principles commented in the introduction.

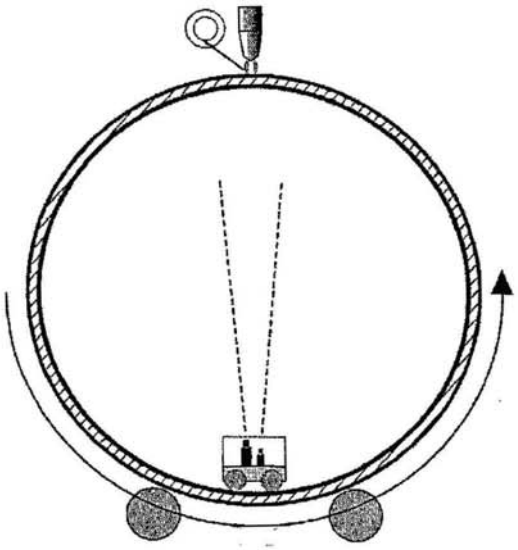

Fig. 1. Schematic view of the submerged arc welding (SAW) process of steam generators for the nuclear industry. The welding torch (top) remains fixed while the entire generator is rotated.

With this particular arrangement, back-face imaging of the welding pool and HAZ is a promising approach. It must be noted that manual monitoring by an operator from the outside is not possible, while an inspection from the inside has severe safety concerns, especially during the welding of the last section (final joint), for which the access to the interior of the generator is restricted to a manhole.

In the next section, the proposed principle of monitoring, which is aimed at the prevention of the perforation defect, will be detailed.

3. BACK-FACE IMAGING WITH THERMAL AND VISIBLE CAMERAS

The aim of the proposed monitoring technique is the prevention of the most occurring defect in this procedure: a perforation of the previously-deposited weld seams. The proposed technique tries, on one hand, to prevent the occurrence of this defect by means of the real-time monitoring of the back-face temperature profile, which should be constant during each welding pass; and on the other hand, to detect a possible perforation in real-time so the process can be stopped and the defect properly re-worked.

The proposed technique is based on the far-field direct observation of the heat affected zone at the back-face of the welding pool, using a thermographic camera. The real-time processing of the images can extract the desired information, namely, the thermal profile of the HAZ (which should be constant in temperature values and shape for each welding pass), and the occurrence of a perforation. From the thermal profile changes, a control action can be derived to prevent the occurrence of a perforation, for example, a change in the travel speed of the piece with respect to the welding torch.

For these tasks (detecting changes in the thermal profile to avoid perforation, and detecting the occurrence of the defect), a simple image analysis technique is proposed: the measurement of the point of maximum temperature, as a rough indication of the stability of the overall thermal profile.

However, one important aim of this work is the feasibility of using a conventional color CCD camera. This is motivated by the high cost of infrared thermographic cameras, compared to CCD cameras in the visible range. Although low-cost infrared cameras are currently available, they are usually restricted in terms of resolution, noise, video interface, or working temperature range of the electronics. Furthermore, as the expected temperatures to be monitored are above 1000K, there is significant radiation within the wavelength detection range of conventional RGB CCD cameras, thus allowing an intensity-based or colorimetric approach to estimate the temperature or the shape of the HAZ at the back-face. Alternatively, a morphological analysis of the visible images is proposed. For a correct welding, isothermal lines in the image are supposed to have a slightly oval shape, which can be approximated by a circle. The radius of the circle should be constant during a correct welding, with a perforation producing a major disruption in the image that is easily detected: both a change in the shape of the weld pool and light coming from the arc plasma emission should be observed.

All the in-lab experimental works carried out to check the proposed techniques have been performed simultaneously with a thermographic and a visible CCD camera, as detailed in the next Section.

4. IN-LAB EXPERIMENTAL SETUP

Several welding experiments under controlled conditions have been carried out in the laboratory. The experimental setup tries to match the setup and environment of welding procedures of the steam generators as much as possible. The experimental setup is shown in Figure 2. Due to inherent restrictions of the lab environment, a Tungsten Inert Gas (TIG) procedure has been employed, using a "Kemppi MasterTIG 2200" power supply with arc current up to 220A. A non-consumable electrode (Tungsten, 1mm diameter) and a supply of shielding gas (Argon, flow of 12L/min) are the main differences with the SAW process, which nonetheless are not expected to affect the suitability of the proposed technique. Plates to be welded were placed in a PC-controlled two-axis linear stage, so any desired trajectory for the weld seam could be performed.

The welding procedure has been observed with two cameras placed side by side two meters away from the welding torch, orthogonal to the back-face of the plates to be welded. At such distance, the parallax error between the images from both cameras can be neglected. The thermographic camera is a CMT-128 from Thermosensorik, configured with a resolution of 128x128 and up to 880 frames per second (fps). Its spectral range covers from 3.4 to 5.1μm. The color CCD camera is an AVT Guppy F-033C from Allied Vision Technologies, configured with 320x240 resolution, 30 fps. A neutral filter was used to prevent saturation of the CCD camera.

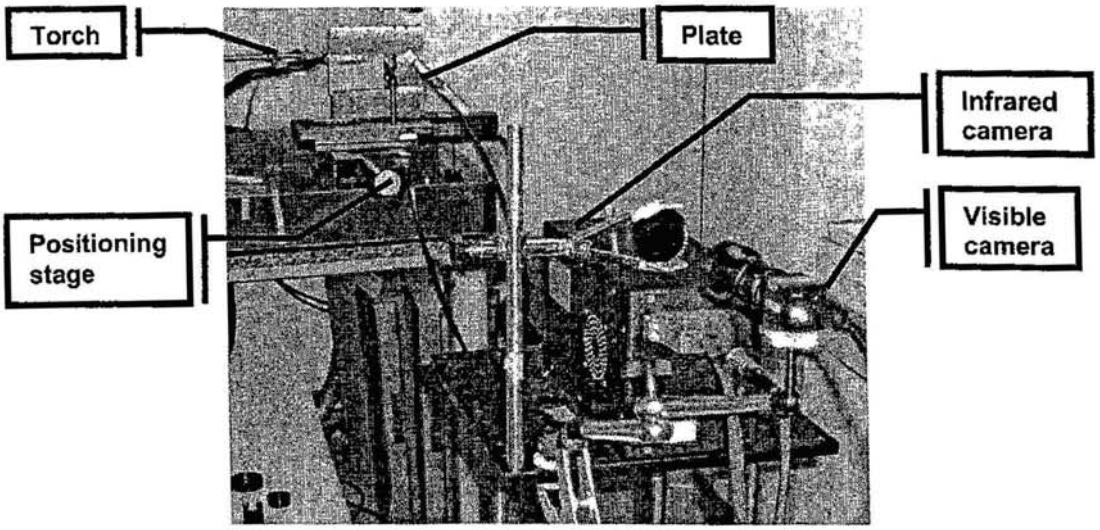

Fig. 2. Experimental setup to perform welds in controlled conditions.

A total number of 27 welding experiments, using the TIG torch in continuous (i.e., non pulsed) mode, have been realized. The material of the plates was stainless steel (AISI 304) of different thickness (1, 2 and 3mm). In order to reproduce the defect of perforation, some of the plates have an incision, a small zone with a reduced thickness in the path of the weld seam. This arrangement tries to simulate the real origin of the perforation defect, which is commonly related to small deviations of thickness of the preliminary weald seam deposited at the inner surface of the shell joints of the steam generator. In Figure 3, a photograph of the resulting welding seams of two relevant experiments is shown. Weld seam labeled "A" (upper part of the photograph) has no defect at the incision, while the weld seam "B" has a clear perforation.

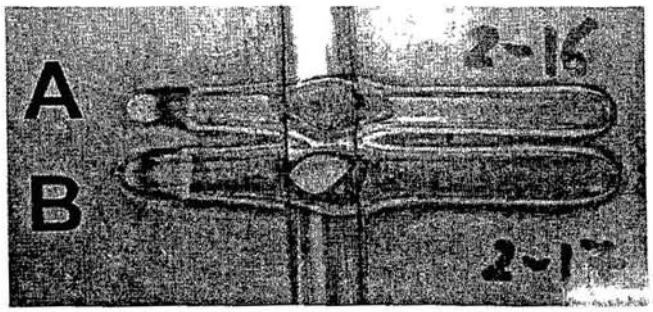

Fig. 3. Photograph of two weld seams without (upper one, labeled "A") and with a perforation defect (labeled "B"). The vertical lines are the edges of the zone with reduced thickness.

Images of the back face of the plate during welding, with both infrared and visible cameras, have been recorded. In the next Section, the results from the image processing algorithms are showed and discussed.

5. RESULTS AND DISCUSSION

5.1 Thermographic imaging

Using the thermographic camera, a sequence of infrared images has been recorded for each welding experiment. For every image, the point of maximum temperature has been located, and its intensity averaged over a 4x4 pixels region.

The temperature of this point is expected to be constant during a correct welding. For plates with different thickness along the seam, which is the case of the two welding experiments shown in this paper, the temperature is expected to be correlated with the plate thickness at every point, provided that the rest of the parameters remain constant. If a perforation occurs, some detectable instability of the maximum temperature is expected.

Figure 4 shows the temporal evolution of the maximum temperature point along the weld seam "A" (upper welding seam of figure 3). The thermal images at some points of the seam are also displayed. It must be noted that the thermal images are not calibrated with a known reference temperature, so the pixel values of the images are the raw amount of infrared radiation detected by the camera, which in turn can be related to the real temperature. This is not an obstacle for the proposed technique because only relative changes of the temperature are analyzed.

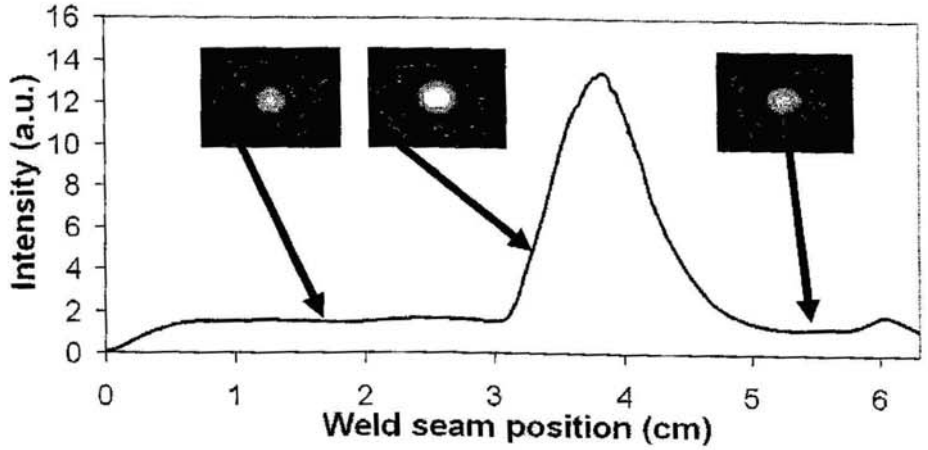

Fig. 4. Evolution of the maximum temperature point along a weld seam "A" with no defects but a zone of reduced thickness. Vertical axis is the total amount of infrared radiation.

It can be seen in Figure 4 zones with different amount of infrared radiation, and thus different temperatures. At the beginning of the weld seam, heating of the back surface from ambient temperature is expected, while at the end (6cm from the origin), the slight increase is provoked because the plate movement stops before the arc is extinguished. Apart from these effects, the temperature remains constant from positions 1cm to 3cm and from 5cm to 6cm, which correspond to a correct welding with constant parameters and plate thickness, as expected. From positions 3cm to 5cm, corresponding to the incision with reduced thickness, an abrupt change in temperature is detected. In this experiment, however, no perforation was observed, but the temperature increment is consistent with the thickness change, as the weld pool approach the back-face of the plate at the incision.

Being one aim of this work the monitoring and control of the welding process in order to avoid the occurrence of defects, in particular perforations, this signal extracted from the infrared image can be used for this task: once the maximum temperature rises above the expected value for a concrete set of process parameters (welding current and speed, material and thickness, ...), a control action, like increasing the welding speed, can be implemented. Typical welding speed in these large structures is quite slow (about 0.5m/min), so no high-speed cameras or signal processing schemes are needed.

Figure 5 corresponds to another welding experiment (weld seam "B"), which resulted in a perforation defect at the incision. In this case, the temporal evolution of the temperature is similar to the previous case, with only a subtle difference: a small instability during the formation of the perforation, which can be seen between positions 3.5cm and 4cm of the weld seam in the Figure.

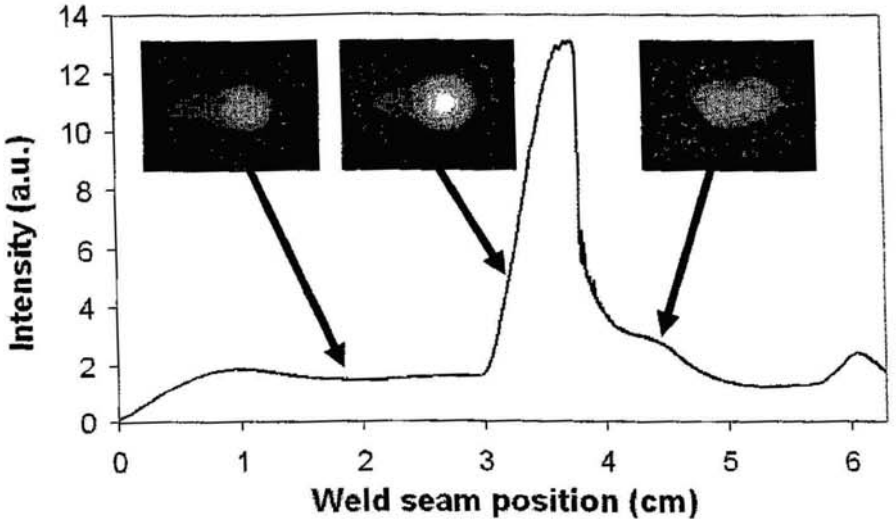

Fig. 5. Evolution of the maximum temperature point along a weld seam "B" with defect of perforation at the incision.

It must be noted that these instabilities of the maximum temperature have been reproduced in all the welding experiments resulting in perforation, so a statistical analysis of the signal reproduced above could alert the occurrence of this defect. However, it is clear from the figure the small amplitude of these instabilities, which could be obscured by noise, especially in a production environment characterized by high levels of electromagnetic interferences. For this reason, another processing scheme, to substitute or complement the above presented, is desirable. In the next paragraphs, an alternative technique based on morphological analysis of the images, is presented. It can be applied to both infrared and visible images, but similar performance is expected in both cases. This is because, as mentioned before, typical working temperatures of the back-face result in significant radiation in the detectable range of common silicon-based CCD cameras, and captured images with both types of camera are quite similar. Only the results with a visible camera are detailed in the following lines.

5.2 Visible imaging

Visible images of each welding experiments have been recorded with the CCD camera. They are synchronized with the thermographic images, so the correlation between them can be used to establish the feasibility of using the visible camera to monitor the behavior of the welding.

Figure 6 shows a sequence of images from the welding experiment "B" commented above, with a perforation defect. Several preliminary conclusions can be extracted from those images. First, the zone of reduced thickness (incision) appears as a brighter, larger spot in the images, with respect to the rest of the seam. The changes in the colors of the spot are also detectable, in response to the wavelength shift of the black body radiation.

Second, the formation of the defect is clearly visible because the radiation from the plasma passes through the void and is captured by the camera. This bright radiation easily saturates the camera, as has happened in this experiment. Additionally, as the main wavelengths emitted by the plasma are located at the short end of the visible spectrum (from near ultraviolet to blue), this is a clear departure from the red dominant images of the incandescent plate surface.

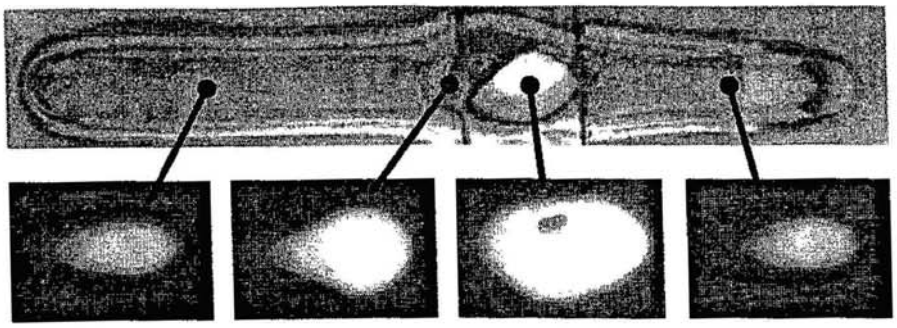

Fig. 6. Visible images taken at different points of the welding experiment, correlated with a photograph of the weld seam.

These facts suggest that temperature estimation and defect detection from visible images could be addressed in two ways: a colorimetric approach (colors of the spot) and a morphological one (size of the spot). However, preliminary experimental results with the available CCD camera suggest that the colorimetric approach does not deliver the required performance. Temperature changes are associated with changes in the overall radiation that easily take the images from under-exposure to saturation. An automatic gain control (AGC) procedure would solve this problem, but its time response, which is usually slow, could be a problem. Additionally, the limited wavelength response and the low intra-image dynamic range associated with color CCD cameras make the imaging of the entire HAZ very difficult, and only a small area around the maximum temperature point can be measured in a reliable way. What is most important, the facts that the significant wavelengths at the working temperatures are limited to the red (R) channel and the expected changes in chromaticity are limited; that there is an inherent noise associated with the CCD imaging, and that the resolution of the R channel is 8 bits only in our case, make it very difficult to measure small changes in temperature with this approach.

This has been experimentally confirmed by means of a black-body calibrator Mikron M330. Images of its surface, at different temperatures, were taken with the CCD camera. The images were averaged and the color parameters extracted. The results are shown in Table 1.

Table 1. Color parameters of images taken by a CCD camera of the surface of a black body calibrator.

	Color value			
Temperature	Hue (0..360°)	Saturation (0..100%)	Luminance (0..100%)	Comments
900°C	0	100	2	Under-exposed
950°C	**19**	**66**	**15**	
1000°C	**22**	**79**	**26**	
1050°C	**23**	**88**	**43**	
1100°C	**24**	**89**	**76**	
1150°C	**37**	**88**	**99**	
1200°C	60	75	100	Over-exposed

It can be seen from the table that the valid analysis range with this particular setup extends from 950°C to 1150°C, a 200°C span. For lower temperatures the amount of visible radiation is very low, while higher temperatures produce saturation of the CCD elements (no automatic gain control –AGC- has been used). Within the useful range of the CCD, it is expected that the Hue value changes linearly with the temperature. Although a monotonic increment is shown, variation range is very small. The data suggest that changes in temperature of less than 50°C are difficult to observe, which is not practical for this application.

For that reason, a morphological analysis is proposed to process the visible images and detect both changes in temperature and the occurrence of the perforation defect, by means of simple shape analysis. The proposed algorithm is shown in Figure 7.

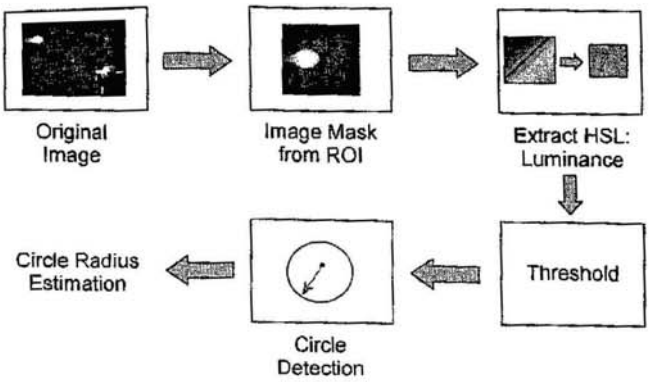

Fig. 7. Algorithm for morphological analysis of the visible images.

It is based on the detection of a circle of luminance around the point of maximum temperature. To do that, several stages are needed: selection of a region of interest (ROI) around the HAZ, conversion of the image to a Hue-Saturation-Luminance (HSL) color model and extraction of the luminance (L) plane, application of a threshold filter, and circle detection. A circle has been selected because the isothermal lines near the maximum temperature point can be considered circular. The radius of the circle is expected to be constant during a correct welding, and change according to temperature changes. In the event of a perforation, an abrupt change in shape is expected, that should be detected by the circle detection algorithm.

This approach has been successfully validated. An example of the results is shown in Figure 8, where the proposed algorithm has been applied to visible images of the welding experiment "B" already described. Changes in circle's radius at the incision (temperature change, image c) in the figure) and in shape during a perforation (image e) in the figure) are clearly detected.

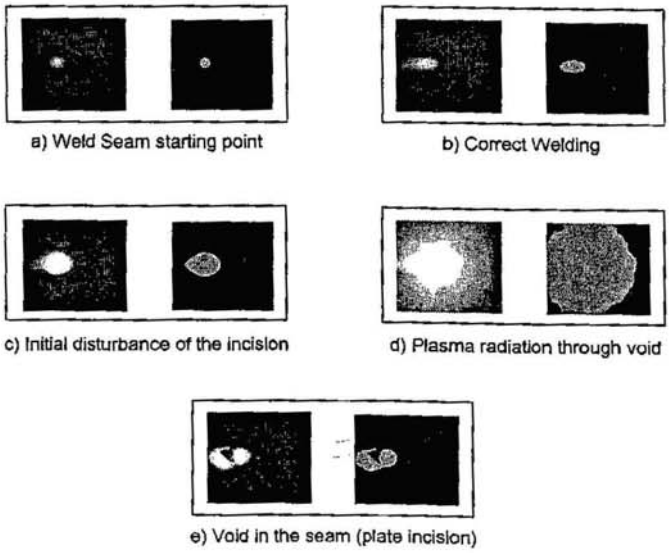

Fig. 8. Example of results of the proposed algorithm for morphological analysis of visible images. Changes in the radius of the circle at the incision and in shape during a perforation are clearly visible.

Finally, as a summary of this section, a comparison of the capabilities of these techniques for welding process control and defect detection, using both infrared and visible images, is presented.

5.3 Comparison of the proposed techniques for infrared and visible images

The main results of this work are summarized in Figure 9. The left part of the figure shows a welding experiment ("A"), where a section of the seam has a reduced thickness that should be detected as an increment in the measured temperature, but no perforation defect was produced. In the right column of the Figure, weld seam "B" shows a clear perforation at the incision.

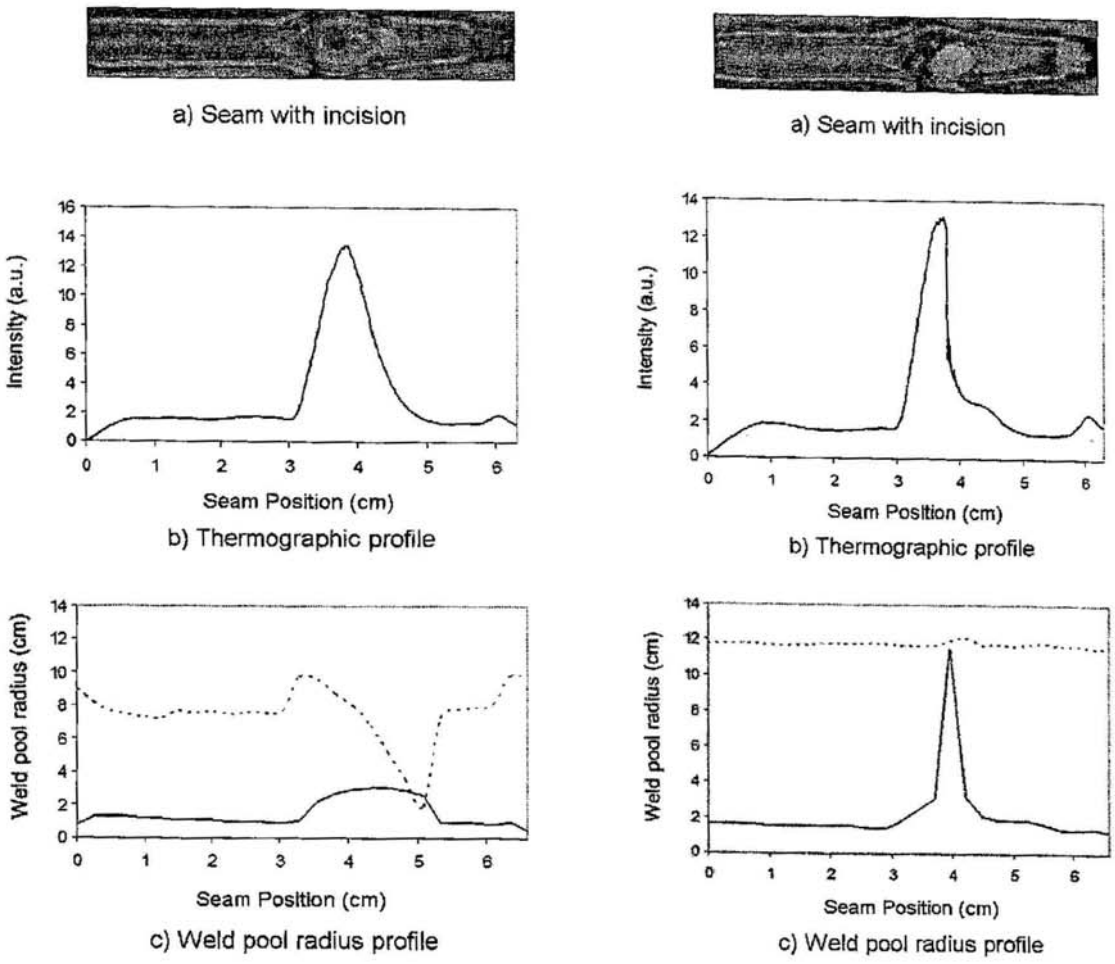

Fig. 9. Summary of the results with the proposed techniques for both infrared and visible imaging of the back surface of the plate under welding. A welding experiment without (left) and with (right) perforation defect is shown. Graphs b) correspond with an estimated maximum temperature from the thermographic images, while graphs c) show a morphological analysis of the visible images. In both cases, the temperature increment of a reduced thickness zone is successfully detected, and also the occurrence of a perforation defect could be derived from the charts.

For the left column (no defect), the tracking of the maximum temperature point of the thermographic image is shown in chart b). The vertical axis is the total infrared radiation captured by the camera, proportional to the temperature, but no temperature calibration has been performed during the experiment. The weld seam position with an important increment of temperature is associated with the position of reduced thickness of the plate. The chart corresponding to the welding experiment with perforation -right column, chart b) – shows a similar behavior, but small instabilities are visible when the perforation occurs.

From the visible images, the shape of a small portion of the heat affected zone, around the maximum temperature point, has been analyzed. After a thresholding operation on the luminance of the visible image, it is fitted to a circle, and its

radius and position recorded. This approach is in fact equivalent to estimate the size position of an arbitrary isothermal from a thermographic image.

Chart c) of the left column of the figure shows the results with no perforation defect: there is an increment of the estimated radius (solid line), resulting from the increased temperature at the incision. The position of the circle within the image (dotted line) varies at the incision, possibly due to the thermal diffusion change at the abrupt thickness changes. For the welding experiment with defect -right column, chart c)-, the radius has a large change when the perforation occurs, due to the change in shape and the irruption of the plasma emission from the arc.

These experimental results show that both approaches are suitable, on one hand, to detect unexpected changes in temperature that can trigger a control signal (like increasing the welding speed) to avoid a possible perforation. On the other hand, once a perforation appears, both techniques are able to detect it, so the process can be stopped and the defect reworked.

6. CONCLUSIONS

In this paper, a technique for control and defect detection of the submerged arc welding process has been presented. It is based on back-face imaging with a thermographic camera and a simple processing scheme to estimate the maximum temperature point. With this approach, the temporal evolution of the plate temperature can be tracked, unexpected changes can be detected, and a control signal could adjust the process parameters (i.e. welding speed) to avoid the occurrence of defects. The most important defect to be detected, the perforation of previously deposited weld seams, can be identified from instabilities shown in the temperature measurement.

Additionally, one important goal of this work has been to study the feasibility of using visible CCD cameras to estimate the temperature and to detect the perforation defect. This was motivated by the much lower cost of visible silicon-based CCD cameras. A colorimetric approach (i.e. the estimation of the temperature by means of the color analysis of the visible images) has been tested and preliminary discarded due to the poor performance of the CCD camera in terms of dynamic range and color resolution. However, a morphological analysis of the visible images has proven to offer the required information about temperature changes and perforation detection.

These techniques for both infrared and visible imaging of the back surface of the plate under welding have been experimentally tested in the laboratory. Several welding trials have been performed in stainless steel plates with changes in thickness to induce temperature variations that could lead to the occurrence of a perforation.

For every welding experiment, a thermographic camera and a CCD color camera recorded simultaneously images of the plate back surface. The analysis of these images confirms the feasibility of the proposed techniques. From the thermal images, the estimation of the temperature of the surface is straightforward: a simple tracking of the point of maximum temperature along the weld seam allows deriving the required control signals to avoid temperature changes that could result in defects. In the event of a perforation, small instabilities are shown in the temperature estimation for all experiments, which could signal the occurrence of this defect.

For the visible images, a morphological analysis by fitting a thresholded image of the heat affected zone to a circle has been performed. As expected, the radius of this circle is related to the temperature, so the tracking of the circle radius and position has allowed the measurement of temperature changes and the occurrence of a perforation.

There are some ongoing works that try to overcome some of the limitations found with the proposed techniques. First, a careful analysis of the colorimetric approach feasibility for temperature estimation using color CCD cameras is being performed. With the help of a black body calibrator, alternative CCD cameras with improved dynamic range and color resolution are being tested. Additionally, temperature referencing of the thermographic camera is being addressed. With these improvements, a precise comparison between infrared and visible images could be performed.

Finally, in-field testing of the proposed techniques for the monitoring and control of the SAW process in the manufacturing of steam generators has already started. The main difficulty is associated with the harsh manufacturing environment: as the cameras and processing equipment have to be placed inside the generator, fumes and projections from the welding process in the event of a perforation, and high temperatures (above 50°C) are expected. Preliminary imaging with a field-capable ThermaCAM SC2000 (from FLIR Systems) suggests that the in-lab results are quite applicable.

ACKNOWLEDGEMENTS

This work has been co-supported by the Spanish TEC'2004-05936-C02-02 and TEC'2005-08218-C02-02 projects. Authors would like to thanks to the staff of the company ENSA (Equipos Nucleares, S.A.) for their assistance.

REFERENCES

1. Li L, Brookfield DJ and Steen WM 1996 Plasma charge sensor for in-process, non-contact monitoring of the laser welding process, *Meas. Sci. Tech.* 7(4) 615-26.
2. Luo H, Zeng H, Hu L, Hu X and Zhou Z 2005 Application of artificial neural network in laser welding defect diagnosis, *Journal of Material Processing Technology* 170 403-11.
3. Sung-Hoon B, Min-Suk K, Seong-Kyu P, Chin-Man C, Cheol-Jung K and Kwang-Jung K 2000 Auto-focus Control and Weld Process Monitoring of Laser Welding using Chromatic Filtering of Thermal Radiation, *Meas. Sci. Tech.* 11 1772-77.
4. Ancona A, Lugara PM, Ottonelli F and Catalano IM 2004 A sensing torch for the on-line monitoring of the gas tungsten arc welding process of steel pipes, *Meas. Sci. Tech.* 15 2412-18.
5. H.C. Wikle III, S. Kottilingam, R.H. Zee, B.A. Chin, "Infrared sensing techniques for penetration depth control of the submerged arc welding process", *Journal of Materials Processing Technology*, Vol. 113, N° 1-3, pp. 228-33, 2001.
6. N.K. Ravala, H. Fan, H.C. Wikle III, B.A. Chin, "Modeling and sensing for penetration control of the saw process in the presence of welding perturbations", *Proceedings of the ASME Heat Transfer/Fluids Engineering Summer Conference 2004*, HT/FED 2004, Vol. 3, pp. 945-52, 2004.
7. B. A. Chin, N. H. Madsen, J. S. Goodling, "Infrared thermography for sensing the arc welding process", *Weld. J.*, Vol. 62, pp. 229-34, 1983.
8. A. Bicknell, J. S. Smith, J. Lucas, "Infrared sensor for top face monitoring of weld pools", *Meas. Sci. Technol.*, Vol. 5, pp. 371-378, 1994.
9. P. Banerjee, S. Govardhan, H.C. Wikle, J.Y. Liu, B.A. Chin, "Infrared sensing for on-line weld geometry monitoring and control", *Journal of Engineering for Industry, Transactions of the ASME*, Vol. 117, N° 3, pp. 323-30, 1995.
10. M.K. Jeon, W.B. Kim, G.C. Han, S.J. Na, "Study on heat flow and temperature monitoring in the laser brazing of a pin-to-plate joint", *Journal of Materials Processing Technology*, Vol. 82, N° 1-3, pp. 53-60, 1998.
11. D.C. Lim, Y.B. Cho, D.G. Gweon, "Robust in-process monitoring of pulsed laser spot welding using a point infrared sensor", *Proceedings of the Institution of Mechanical Engineers, Part B: Journal of Engineering Manufacture*, Vol. 212, N° B3, pp. 241-50, 1998.
12. J.L. Doong, C.S. Wu, J.R. Hwang, "Infrared temperature sensing of laser welding", *International Journal of Machine Tools & Manufacture*, Vol. 31, N° 4, pp. 607-16, 1991.
13. A. Al-Habaibeh, F. Shi, N. Brown, D. Kerr, M. Jackson, R.M. Parkin, "A novel approach for quality control system using sensor fusion of infrared and visual image processing for laser sealing of food containers", *Measurement Science and Technology*, Vol. 15, N° 10, pp. 1995-00, 2004.
14. G. Qin, X. Qi, Y. Yang, X. Wang, S. Lin, "Coaxial visual sensing technology in Nd:YAG laser welding with high power", *Chinese Journal of Mechanical Engineering*, Vol. 40, N° 7, pp. 180-85, 2004.
15. G. Qin, S. Lin, "Weld penetration monitoring in ND:YAG laser deep penetration welding based on coaxial visual sensing technology", *Chinese Journal of Mechanical Engineering*, Vol. 42, N° 8, pp. 229-33, 2006.
16. F. Bardin, S. Morgan, S. Williams, R. McBride, A. Moore, J. Jones, D. P. Hand, "Process control of laser conduction welding by thermal imaging measurement with a color camera", *Applied Optics*, Vol. 44, n 32, Nov 10, 2005, pp 6841-6848.
17. W. Chen, X. Zhang, L. Jia, Y. Pu, "Penetration monitoring and control of CO2 laser welding with coaxial visual sensing system", *Proceedings of SPIE - Lasers in Material Processing and Manufacturing II*, Vol. 5629, pp. 129-40, 2005.
18. R. Kovacevic, Y.M. Zhang, S. Ruan, "Sensing and control of weld pool geometry for automated GTA welding", *Journal of Engineering for Industry, Transactions of the ASME*, Vol. 117, N° 2, pp. 210-22, 1995.
19. J.S. Smith, W. Lucas, "Vision based control of arc welding processes", *Welding in the World, Le Soudage Dans Le Monde*, Vol. 46, N° SPEC, pp. 251-62, 2002.